7800–7813 *Nucleic Acids Research, 2010, Vol. 38, No. 21* *Published online 21 July 2010*
doi:10.1093/nar/gkq641

A molecular clamp ensures allosteric coordination of peptidyltransfer and ligand binding to the ribosomal A-site

Arturas Meskauskas[1,2,*] and Jonathan D. Dinman[1,*]

[1]Department of Cell Biology and Molecular Genetics, University of Maryland, College Park, MD 20742 and [2]Department of Biotechnology and Microbiology Vilnius University, Vilnius, LT 03101, Lithuania

Received June 3, 2010; Revised July 1, 2010; Accepted July 2, 2010

ABSTRACT

Although the ribosome is mainly comprised of rRNA and many of its critical functions occur through RNA–RNA interactions, distinct domains of ribosomal proteins also participate in switching the ribosome between different conformational/functional states. Prior studies demonstrated that two extended domains of ribosomal protein L3 form an allosteric switch between the pre- and post-translocational states. Missing was an explanation for how the movements of these domains are communicated among the ribosome's functional centers. Here, a third domain of L3 called the basic thumb, that protrudes roughly perpendicular from the W-finger and is nestled in the center of a cagelike structure formed by elements from three separate domains of the large subunit rRNA is investigated. Mutagenesis of basically charged amino acids of the basic thumb to alanines followed by detailed analyses suggests that it acts as a molecular clamp, playing a role in allosterically communicating the ribosome's tRNA occupancy status to the elongation factor binding region and the peptidyltransferase center, facilitating coordination of their functions through the elongation cycle. The observation that these mutations affected translational fidelity, virus propagation and cell growth demonstrates how small structural changes at the atomic scale can propagate outward to broadly impact the biology of cell.

INTRODUCTION

Analyses of a growing number of high resolution ribosome structures coupled with kinetic studies are revealing that the ribosome is highly dynamic, capable of assuming >40 different conformational states through the translation elongation cycle [reviewed in (1)]. Thus, a critical question is how the ribosome coordinates all of these states to ensure the directionality and fidelity of protein synthesis. The general answer lies in allostery: the formation and breaking of specific intermolecular contacts in response to different ligand binding states serves as a series of switches to ensure that the ribosome is optimally configured to proceed to the next functional state. The current challenge is to identify and functionally map the specific allosteric switching components.

Numerous researchers have employed elegant biochemical, biophysical, structural, genetic, and computational approaches to this problem, a few of which are highlighted here. For example, biochemical approaches have been employed to define the kinetic parameters governing every step of the elongation cycle, revealing that selection of the appropriate aminoacyl–tRNA (aa-tRNA) depends on a two step kinetic process [reviewed in (2)]. Biophysical methods have revealed that conformational switching by rRNA and ribosomal protein L1 ensures exit of deacylated tRNA from the ribosome (1,3), while real time single molecule fluorescence and force measurements are revealing dynamic motions of the ribosome and tRNAs, and directly probing the forces stabilizing ribosomal complexes [reviewed in (4)]. Biochemical, computational and high resolution structural methods have been employed to map changes in rRNA structures during the transit of tRNAs through the ribosome and during the peptidyltransfer reaction (5–10). Pertinent to this study, we have previously used a combination of molecular genetics, biochemical and biophysical approaches to identify the contributions of specific ribosomal proteins and rRNA bases involved in coordinating the stepwise process of accommodation of aa-tRNA into the ribosomal A-site, activation of the peptidyltransferase center, and recruitment of the trans-acting translocase (EF-G in bacteria, eEF2 in eukaryotes) using yeast ribosomes as a model (11–16).

*To whom correspondence should be addressed. Tel: +1 301 405 0981; Fax: +1 301 314 9489; Email: dinman@umd.edu
Correspondence may also be addressed to Arturas Meskauskas. Tel: +1 301 405 6030; Fax: +1 301 405 0745; Email: artmeska@umd.edu

Ribosomal protein L3 in particular appears to have an important function in this process. Figure 1A shows L3 within the context of the large ribosomal subunit (LSU), including the following structural and functional elements; the peptidyltransferase center (PTC), the aa-tRNA accommodation corridor which lies in between Helix 89 and the complex Helix 90–92 structure, Helix 95 (the Sarcin/Ricin Loop or SRL), and the GTPase-associated center (GAC). The latter two structures interact with the eEF1A–aa-tRNA–GTP ternary complex and eEF2 (the eukaryotic translation elongation factor homologs of bacterial EF–Tu-aa-tRNA–GTP ternary complex and EF-G, respectively). The 3D rendering in Figure 1B shows that L3 contains a globular domain that interfaces with the solvent side of the LSU, and two structures, the N-terminal extension and a central loop that extend deep into the central core of the LSU. The central loop can be subdivided into two domains, the 'tryptophan finger' (W-finger) positioned at the tip of the central extension, and a cluster of basic amino acids that protrudes from the center of the internal loop like a thumb roughly perpendicular to the W-finger that we call the L3 'basic thumb'. Figure 1C shows that this basic thumb is nestled in the core of a cagelike structure formed by elements of three different 25S rRNA helices: H61, H73 and H90. We previously proposed a 'rocker switch' model describing how structural rearrangements of the N-terminal extension and the W-finger of L3 function to coordinate the stepwise processes of translation elongation (17). Missing from the prior analyses was an explanation of how the movements of these extensions of L3 are communicated to functional centers of the ribosome. In this current study, analysis of the basic thumb of L3 illuminates this question. Mutagenesis of the indicated amino acids to alanines followed by genetic, biochemical and structural analyses suggests that the basic thumb acts as a molecular clamp to play a role in allosterically communicating the ribosome's tRNA occupancy status to the elongation factor binding region and the peptidyltransferase center, thus facilitating coordination of their functions through the elongation cycle.

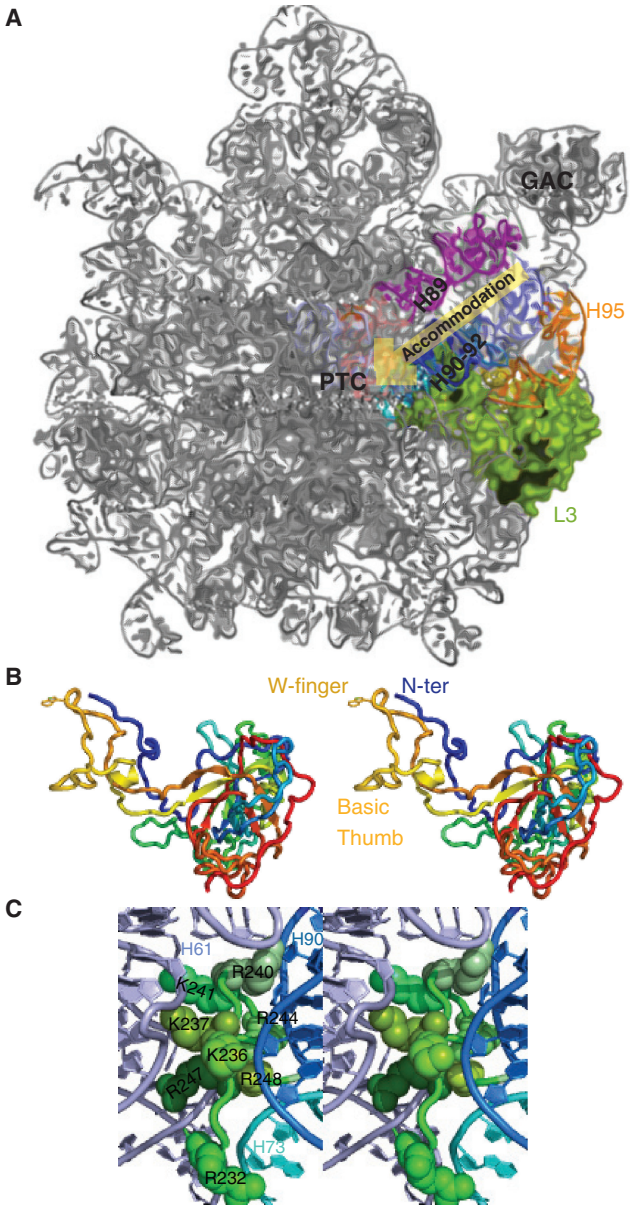

Figure 1. The L3 basic thumb. (**A**) Crown view of the yeast 60S subunit from (36). L3 is indicated in green. The aa-tRNA accommodation corridor is framed by Helix 89, and the complex structure formed by Helices 90–92. Elongation factors bind to the GTPase Associated Center (GAC) and the Sarcin/Ricin Loop (SRL) at the tip of Helix 95. The peptidyltransferase center (PTC) is in the center of the large subunit. (**B**) The 3D view of isolated L3, heat map colored from the N-terminus (blue) to the C-terminus (red). The N-terminal extension and the basic thumb and tryptophan (W) finger of the central extension are indicated. (**C**) The 3D view of interactions between amino acid residues of the L3 basic thumb investigated in this study. It is surrounded by a cagelike structure formed by 25S rRNA Helices 61–64, H73 and H90. Amino acids mutated in this study are labeled.

MATERIALS AND METHODS

Strains, plasmids, genetic manipulation and media

Escherichia coli DH5α was used to amplify plasmid DNA. Transformation of *E. coli* and yeast, and preparation of yeast growth media (YPAD, synthetic drop out medium, and 4.7 MB plates for testing the Killer phenotype) were as reported earlier (18). Restriction enzymes were obtained from MBI Fermentas (Vilnius, Lithuania). The QuikChange XL II site-directed specific mutagenesis kit was obtained from Stratagene (La Jolla, CA, USA). Macrogen Inc. (Piscataway, NJ, USA) performed DNA sequence analysis. Oligonucleotide primers were purchased from IDT (Coralville, IA, USA). The yeast strains used in this study were all derived from the *rpl3*-gene disruption (*rpl3Δ*) strain JD1090 (*MATα ura3-52 lys2-801 trp1δ leu2*$^{-}$ *his3 RPL3::HIS3* p*RPL3-URA3-CEN6* [L-A HN M_1]) (19). Mutants of *rpl3* were generated using the wild-type *RPL3* gene in pJD225 (19), synthetic oligonucleotides, and the QuikChange XL II kit. The pYDL dual luciferase reporter series of plasmids for monitoring programmed ribosomal frameshifting (PRF) were used as described earlier (20).

Assays for the killer phenotypes and measurement of frameshifting

The killer virus assay was carried out as described earlier (18). Briefly, yeast colonies were replica plated to 4.7MB plates newly seeded at an optical density at 595 nm (OD_{595}) of 0.5 of the 5×47 killer indicator strain per plate. After 2–3 days at 20°C, killer activity was scored as a zone of growth inhibition around the Killer$^+$ colonies. To monitor programmed −1 frameshifting using the dual luciferase reporter plasmids, glass beads were used to prepare lysates from cells expressing the 0-frame, −1 (L-A derived), or +1 (Ty*1* derived) dual luciferase plasmids (20). After clarification of the lysates by centrifugation, typically 5 µl was used in a total volume of 100 µl of dual luciferase assay reagents (Promega, Madison WI, USA), and *Renilla* and firefly luciferase activities were quantitated using a TD20/20 luminometer (Turner Designs, Sunnyvale, CA, USA). Frameshifting efficiencies were calculated by dividing the firefly/*Renilla* luminescence ratios from lysates of cells expressing the PRF test reporters by the same ratio obtained from lysates of cells expressing the zero-frame control reporter. All assays were replicated enough times to achieve >95% confidence levels, and statistical analyses were performed as described earlier (21).

Synthesis of aminoacyl–tRNA and acetylated aminoacyl–tRNA

Aminoacyl–tRNA synthetases were purified as described earlier (22,23).Yeast $tRNA^{Phe}$ was aminoacylated with unlabeled phenylalanine or with [^{14}C]Phe to make Phe-$tRNA^{Phe}$ and [^{14}C]Phe-$tRNA^{Phe}$, respectively. [^{14}C]Phe-$tRNA^{Phe}$ was used to monitor enzymatic binding to the A site of poly(U) primed ribosomes, and acetylated-[^{14}C]Phe-$tRNA^{Phe}$ (Ac-[^{14}C]Phe-$tRNA^{Phe}$) was generated to monitor nonenzymatic P-site binding using poly(U) primed salt washed ribosomes. Phe-$tRNA^{Phe}$ and Ac-Phe-$tRNA^{Phe}$ were used in SHAPE structure probing experiments (see below). Yeast $tRNA^{Phe}$ was aminoacylated as described earlier (24) with minor modifications. The reaction mix (1 ml) contained 100 mM HEPES–KOH, pH 7.6, 10 mM KCl, 20 mM $MgCl_2$, 10 mM ATP, 100 µM [^{14}C]Phe [496 mCi/mM], 1 mM DTT, 2000 U pyrophosphatase (Sigma), plus 0.2 mg of $tRNA^{Phe}$ and 40 µl of aminoacyl–tRNA synthetases. Reaction mixtures were incubated for 30 min at 30°C, and proteins were removed by extraction with acid–phenol–chloroform. Charged tRNAs were ethanol precipitated and purified using G25 spin columns. [^{14}C]Phe-$tRNA^{Phe}$ was separated from uncharged tRNA by high-performance liquid chromatography (HPLC) as described earlier (25) with the following modifications. Samples were loaded onto a 4.6- by 250-mm JT Baker wide-pore butyl column equilibrated with buffer A (20 mM NH_4Cl, 10 mM $MgCl_2$, 400 mM NaCl; pH 5.0) at 1 ml/min. The column was washed with 10 ml of buffer A, conditions under which free phenylalanine and aminoacyladenylate are eluted from the column. Uncharged tRNAs and residual free [^{14}C]Phe and nucleotides were eluted by isocratic elution of 19 ml at 15% of buffer B (20 mM NH_4Cl, 10 mM $MgCl_2$, 400 mM NaCl, 60% methanol; pH 5.0). [^{14}C]Phe-$tRNA^{Phe}$ was eluted using a programmed binary gradient of buffers A and B. Elution of aa-tRNA was monitored by OD_{260} readings, and [^{14}C]Phe-$tRNA^{Phe}$ concentrations and specific activities were determined. The presence of aa-tRNA in the eluted material was confirmed by TLC (24). Ac-[^{14}C]Phe-$tRNA^{Phe}$ was obtained in a similar manner. Yeast $tRNA^{Phe}$ was charged with [^{14}C]Phe as above, extracted with phenol and purified using G25 columns. Reaction mix (4 ml) contained 200 mM NaOAc, pH 5.2 and 7 nmol of [^{14}C]Phe-$tRNA^{Phe}$. Acetylation was carried out by addition of 64 µl of acetic anhydride at 1 h intervals for 2 h on ice. After incubation, NaOAc concentration was raised to 300 mM and Ac-[^{14}C]Phe-$tRNA^{Phe}$ was ethanol precipitated. Ac-[^{14}C]Phe-$tRNA^{Phe}$ was further purified by HPLC as described earlier.

Purification of yeast ribosomes

Sulfolink resin was charged with cysteine as described earlier (26). Yeast cells were grown in YPAD media to mid log phase, collected and washed with binding buffer (10 mM Tris–HCl, pH 7.5; 5 mM $MgCl_2$; 60 mM NH_4Cl; 2 mM DTT). Cells were suspended in binding buffer and disrupted using a Mini Bead Beater. Lysates were centrifuged at 30 000*g* for 30 min in Beckman MLS 50 rotor. Supernatant (2 ml) was removed and added to 2 ml of cystein-charged Sulfolink slurry (50% resin equilibrated with binding buffer) and incubated on ice for 15 min with mixing as resin sediments. After incubation resin was spun down at 1500*g* for 0.5 min. Supernatants were removed and resin washed five times with 5 ml of binding buffer. After washing, resin was suspended in 1 ml of elution buffer (10 mM Tris–HCl, pH 7.5; 10 mM $MgCl_2$; 0.5 M KCl; 1 mg/ml heparin; 2 mM DTT) and incubated for 5 min on ice with occasional mixing. The suspensions were centrifuged, supernatant collected, and elution was repeated two more times. Supernatants were combined (3 ml total volume) and GTP and pH neutralized puromycin were added to 1 mM each. After incubation at 30°C for 30 min, reaction mixtures were loaded on top of a 1 ml glycerol cushion (10 mM Tris–HCl, pH 7.5; 10 mM $MgCl_2$; 0.5 M KCl; 2 mM DTT; 25% glycerol) and centrifuged at 100 000*g* for 16 h. Ribosome pellets were suspended in 2 ml of elution buffer without heparin, loaded on top of 2 ml glycerol cushions and centrifuged at 100 000*g* for 16 h. Ribosome pellets were resuspended in storage buffer [50 mM HEPES–KOH pH 7.6; 5 mM $Mg(CH_3COO)_2$; 50 mM NH_4Cl; 1 mM DTT; 25% glycerol] at 5–10 pmol/µl (1 OD_{260} = 2 pmol) and stored at −80°C.

Characterization of peptidyltransferase activity

Complex C [ribosome-poly(U)-AcPhe-tRNA] was formed in 400 µl of binding buffer (80 mM Tris–HCl, pH 7.4, 160 mM ammonium chloride, 11 mM magnesium acetate, 2 mM spermidine and 6 mM β-mercaptoethanol) containing 0.4 mM GTP, 500 pmol ribosomes, 0.4 mg/ml poly(U) and 700 pmol Ac-[^{14}C]Phe-tRNA. Mixtures were incubated

for 20 min at 30°C and then placed on ice. Complexes were purified from free Ac-[^{14}C]Phe-tRNA^{Phe} by centrifugation through a glycerol cushion (0.5 ml; 20% glycerol in binding buffer by centrifugation at 50 000 rpm for 2 h in MLS 50 rotor). Ribosome pellets were rinsed twice with 1 ml of binding buffer and suspended in 1.15 ml of binding buffer. For puromycin reactions, 1.15 ml of complex C extract was pre-incubated at 30°C for 5 min, and reactions were initiated by adding pH neutralized puromycin (100 mM stock) to final concentrations of 10 mM. Aliquots of 100 µl were removed, and reactions were terminated at the indicated time intervals by addition of 100 µl of 1.0 N NaOH. Reaction products were extracted with 0.4 ml of ethyl acetate, 0.2 ml of organic phase was transferred to scintillation vials, and radioactivity was determined by scintillation counting. A 50-µl aliquot of initial reaction mixture was also transferred to scintillation vials, and total radioactivity (N_o) was determined. Controls without puromycin were included in each experiment, and the values obtained were subtracted as background. The percent of the bound Ac-[^{14}C]Phe-tRNA^{Phe} converted to Ac-[^{14}C]Phe-puromycin was corrected with the extent factor α (determined if complex C were allowed to react for 1 h; $C_o = \alpha N_o$), as described earlier (27,28). The reaction plots were fit to a first-order exponential equation, and values of K_{obs} (the apparent rate constant of entire course of reaction at a given concentration of puromycin) were calculated by using Graphpad Prism software.

aa-tRNA and Ac-aa-tRNA-binding studies

Soluble protein factors were prepared as described earlier (28,29). aa-tRNA binding to the A-site of the ribosome was carried out as described earlier (13). Ribosome mixtures (50 µl) contained 80 mM Tris–HCl, pH 7.4, 160 mM NH_4Cl, 11 mM $Mg(CH_3COO)_2$, 6 mM β-mercaptoethanol, 2 mM spermidine, 0.4 µg/ml of poly(U) and 25 pmol of ribosomes. For A-site-binding experiments, ribosome mixtures were preincubated with uncharged tRNA (4:1 tRNA/ribosomes) at 30°C for 15 min to ensure full occupation of P-sites by uncharged tRNA. [^{14}C]Phe-tRNA^{Phe} /GTP/eEF1A ternary complex was formed by incubating (5 min at 30°C) [^{14}C]Phe-tRNA^{Phe} in binding buffer with 0.4 mM GTP and 10 µg/ml soluble protein factors. The 2-fold dilutions of [^{14}C]Phe-tRNA^{Phe} ternary complex were added to ribosome mix. Reaction mixtures were incubated at 30°C for an additional 20 min to allow formation of [^{14}C]Phe-tRNA^{Phe}-80S-poly(U) complexes. For P-site-binding experiments 2-fold dilutions of Ac-[^{14}C]Phe-tRNA^{Phe} were added to ribosome mixtures and incubated for 20 min at 30°C. Aliquots were then applied onto nitrocellulose membranes, filters were washed with 6 ml of binding buffer, and radioactivity was measured by scintillation counting. Background levels of radioactivity were determined using a blank sample (without ribosomes) and subtracted from test samples. K_d values were determined assuming single binding sites using Graphpad Prism software.

eEF2 binding

6xHis-tagged eEF2 was purified from TKY675 yeast cells (kindly provided by Dr T. Kinzy) as described earlier (30) with the following modifications. EDTA was added to 5 mM to eluted eEF2 just before dialysis to bind leached Ni^{2+} ions and prevent precipitate formation during dialysis due to aggregation of His-tagged protein. eEF2 concentration was determined by [^{14}C]ADP-ribosylation with diphtheria toxin (see below). Each preparation of eEF2 showed linear concentration response curves in the range of eEF2 amounts used in binding experiments. For eEF2-binding experiments, reaction mixes (25 µl) containing 12.5 pmol of salt washed 80S ribosomes and various concentrations of 6xHis-tagged eEF2 in binding buffer (50 mM Tris–HCl, pH 7.5, 50 mM ammonium acetate, 10 mM magnesium acetate, 2 mM DTT, 100 µM GDPNP) were incubated for 20 min at room temperature. Estimation of bound eEF2 was carried out as follows by assuming that ribosome bound eEF2 is not susceptible to ADP-ribosylation by diphtheria toxin (31–33). Free (unbound) eEF2 was estimated by ADP-ribosylation of eEF2: 100 pmol [^{14}C] NAD^+ and 0.2 µg of diphtheria toxin were added to each reaction mix and incubated for 30 min at 30°C. Total eEF2 in each reaction mix was determined by ADP-ribosylation reaction after bound eEF2 was released by adding EDTA to 10 mM. Reaction mixes were precipitated with TCA, and amounts of [^{14}C]ADP-ribosylated eEF2 were determined by liquid scintillation counting. Control values (lacking diphtheria toxin) were subtracted. Ribosome bound eEF2 was calculated by subtracting free values from total amount. K_d values were determined assuming single binding sites using Graphpad Prism software.

SHAPE structure probing of mutant ribosome–tRNA complexes

To prime ribosomes with poly(U), reaction mix (100 µl) in binding buffer (80 mM Tris–HCl, pH 7.4, 100 mM NaCl, 15 mM $Mg(CH_3COOH)_2$, 6 mM β-mercaptoethanol) containing 55 pmol ribosomes and 50 µg poly(U), was incubated for 20 min at 30°C. Next, for P-site complex, 200 pmol of Ac-Phe-tRNA^{Phe} was added. For structure probing of ribosomes with occupied A sites, ribosomal P sites were blocked with 4× excess of deacylated tRNA^{Phe} and Phe-tRNA^{Phe} (200 pmol), GTP (0.5 mM) and 5 µl of crude elongation factor mix were added. Reaction mixes were incubated for 20 min at 30°C. Reactions were divided into two parts of 50 µl each (control and modification tubes) and 75 µl of binding buffer was added to each tube. 25 µl of 1M7 (130 mM in DMSO) was added to modification tubes. Control samples contained 25 µl of DMSO. After incubating for 85 min at 30°C ribosomes were precipitated with 450 µl ethanol. Ribosomal RNA was extracted using RNAqueous kit (Ambion). Pellets were dissolved in 100 µl of RNAqueous Lysis Buffer and processed according manufactures instructions. RNA was eluted in 50 µl volume and concentration adjusted to 1 µg/µl with elution buffer. Reverse transcriptase (RT) primer extension analyses of modified RNAs were performed

as described (34). The site-specificity of charged tRNA binding was confirmed using the puromycin reaction (35).

Computational analysis of ribosome structure

The cryo-electron microscopy (cryo-EM) reconstruction of *Thermomyces lanuginosus* modeled with Saccharomyces cerevisiae rRNA and ribosomal proteins (36) was visualized using PyMOL (DeLano Scientific LLC).

RESULTS

The L3 basic thumb mutants affect cell growth, programmed −1 ribosomal frameshifting and yeast Killer virus maintenance

*rpd3Δ*cells harboring wild-type pRPL3-Ura were transformed with mutant *rpl3* alleles expressed from a low copy *TRP1* vector, and the viability of mutants was assessed by their ability to grow in the presence of 5-FOA. All of the L3 basic thumb single mutants (R232A, K236A, K237A, K241A, R244A, R247A and R248A) were viable as the sole forms of L3 with the exception of R240, which was lethal (Figure 2A, summarized in Table 1). Among the viable single mutants, only R232A and R247A conferred noticeable growth defects. A series of double mutants were constructed based on the viable mutants and their physical locations relative to one another. This analysis revealed that the K236A/R247A and K241A/R244A mutants significantly affected cell growth, while the R247A/R248A mutant was inviable. The K236A/K237A double mutant did not grossly affect cell growth.

Most strains of *S. cerevisiae* harbor a symbiotic virus called 'Killer', a bipartite dsRNA viral system composed of the L-A helper virus and the M_1 satellite [reviewed in (37)]. The 4.6-kb dsRNA L-A viral genome encodes the viral coat protein (Gag), and the Gag-pol replicase that is encoded by a programmed −1 ribosomal frameshift (−1 PRF) (38). The M_1 satellite dsRNA is encapsidated and replicated inside of L-A encoded viral particles. The M_1 encoded preprotoxin is processed by the Kex1p and Kex2p cellular proteases into the mature secreted toxin.

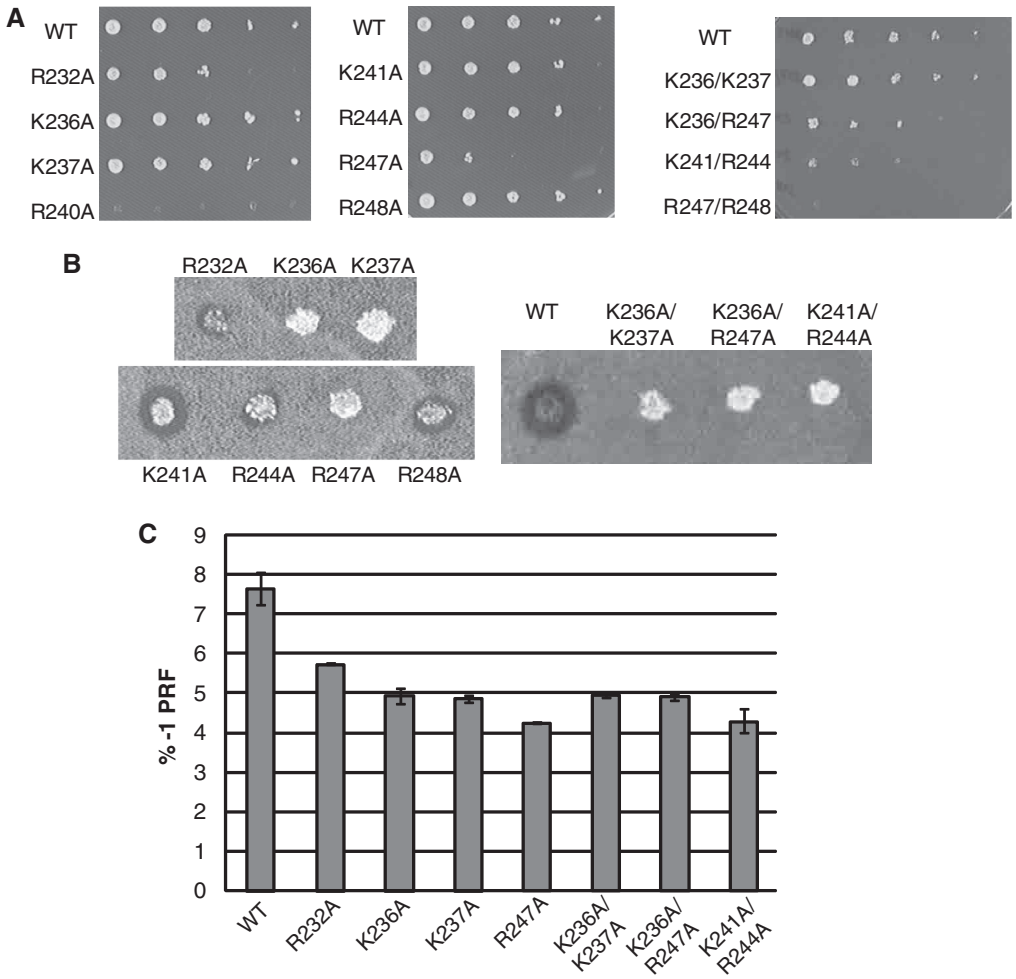

Figure 2. Effects of L3 basic thumb mutants on cell growth, virus propagation and programmed –1 ribosomal frameshifting. (**A**) Ten-fold dilution spot assays ($10^4 \rightarrow 10^0$ CFU) of cell growth at 30°C. (**B**) Killer assay. Cells were replica plated onto a lawn of diploid Killer$^-$ indicator cells and grown at 20°C for 3 days. Zone of growth inhibition indicates presence of the Killer virus. (**C**) Dual luciferase assays were used to measure percent programmed –1 ribosomal frameshifting from an L-A virus derived –1 PRF signal (20;21). Error bars denote standard errors.

Table 1. Summary of L3 Basic Thumb mutants

L3[a]	Growth[b]	Killer[c]	% –1 PRF[d]	A-site (nM)[e]	rRNA SHAPE[f]	% +1 PRF[g]	P-site (nM)[h]	eEF2 (nM)[i]	Puro K_{obs} (min^{-1})[j]
WT	WT	+	7.6 ± 0.4	92.4 ± 10.7	WT	7.4 ± 0.6	72.6 ± 8.3	382.8 ± 93.3	0.34 ± 0.05
R232A	↓↓	w	5.7 ± <0.1	126.3 ± 7.1	PTC	6.6 ± 0.3	74.2 ± 7.1	341.0 ± 115.3	0.22 ± 0.02
K236A	WT	–	4.9 ± 0.2	163.3 ± 11.7	H73, H90, H91, PTC	6.7 ± 0.1	78.4 ± 5.1	312.4 ± 74.4	0.20 ± 0.03
K237A	WT	–	4.9 ± 0.1	167.7 ± 24.8	H73, H91, H92, H94	6.5 ± 0.3	81.2 ± 4.4	341.7 ± 55.9	0.61 ± 0.08
R240A	Lethal	ND	ND	ND	ND	ND	ND	ND	ND
R241A	↓	+	ND	ND	ND	ND	ND	ND	ND
R244A	↓	w	ND	ND	ND	ND	ND	ND	ND
R247A	↓↓↓	–	4.2 ± <0.1	305.7 ± 41.7	H73, H94, H91, PTC, H94, H95	6.0 ± 0.7	73.9 ± 9.4	46.6 ± 26.9	0.23 ± 0.03
K248A	WT	w	ND	ND	ND	ND	ND	ND	ND
K236A/K237A	WT	–	4.9 ± 0.1	244.9 ± 23.3	ND	7.1 ± 0.17	94.9 ± 10.6	84.0 ± 42.3	0.17 ± 0.02
K236A/R247A	↓↓	–	4.9 ± 0.1	272.4 ± 34.4	ND	7.0 ± <0.1	71.3 ± 6.9	110.2 ± 46.2	0.18 ± 0.03
K241A/R244A	↓↓↓	–	4.3 ± 0.3	340.3 ± 39.2	ND	6.5 ± 0.1	84.4 ± 14.8	229.4 ± 71.3	0.14 ± 0.04
R247A/R248A	Lethal	ND	ND	ND	ND	ND	ND	ND	ND

WT denotes wild-type, and ND represents Not Determined.
[a]L3: Version of L3 assayed.
[b]Effects of mutants on cell growth from Figure 1A. Down arrows indicate relative effects observed using 10-fold dilution spot assay.
[c]Data summarized from Figure 1B. + = Wild-type Killer phenotype; w = weak Killer phenotype; – = unable to maintain Killer virus.
[d]% –1 PRF data from Figure 1C with standard error indicated.
[e]Mean and standard deviation K_d values of aa-tRNAs bound to the A-site from Figure 2B.
[f]Summary from Figure 4A of regions in 25S rRNA where changes were observed using SHAPE.
[g]% +1 PRF data, standard error indicated.
[h]Mean and standard deviation K_d values of Ac-aa-tRNAs bound to the P-site from Figure 2D.
[i]Mean and standard deviation K_d values of eEF2 bound to ribosomes from Figure 2F.
[j]Mean and standard deviations of rates of peptidylpuromycin formation from Figure 2H.

Cells infected by L-A and M_1 can kill uninfected cells, but are themselves immune, hence the name 'Killer'. The presence of Killer can be easily assayed by replica plating test cells onto a lawn of diploid uninfected (indicator) cells: Killer$^+$ cells will kill the nearby indicator cells, resulting in a ring of growth inhibition around the test cells. One of the first yeast mutants cloned, *mak8-1*, was first identified by its inability to maintain the killer phenotype (Mak$^-$ phenotype) and encodes an allele of *rpl3* (39). Analyses of the L3 basic thumb mutants revealed that three of the single mutants (K236A, K237A and R247A) were completely unable to maintain the Killer virus, while R232A and R244A had weak Killer phenotypes. None of the double mutants were able to maintain the virus (Figure 2B, summarized in Table 1).

The efficiency of −1 PRF determines the relative ratio of structural Gag to enzymatic Gag-pol available for viral particle self-assembly, and changing −1 PRF strongly inhibits virus maintenance (18,40). Previous studies have identified numerous L3 mutants that promoted altered rates of L-A promoted programmed −1 ribosomal frameshifting (−1 PRF), but did not affect Ty*1* mediated programmed +1 ribosomal frameshifting (+1 PRF) (13,17,19,23). However, while all previous L3 mutants analyzed to date enhanced −1 PRF efficiency, all of the viable L3 basic thumb mutants promoted decreased −1 PRF, ranging between ∼55% and ∼75% of wild-type rates (Figure 2C, summarized in Table 1). The significance of these changes in −1 PRF is confirmed by loss of the Killer virus, maintenance of which is known to be sensitive to even small decreases in −1 PRF rates (18,41). Consistent with prior studies none of the basic thumb mutants affected +1 PRF (summarized in Table 1).

The Killer$^-$ L3 basic thumb mutants affect binding of ligands to the ribosomal A-site and peptidyltransfer

The simultaneous slippage model of −1 PRF requires that both the aa-tRNA in the ribosomal A-site, and the peptidyl–tRNA in the P-site must shift on the mRNA (42), while in Ty*1* mediated +1 PRF, only the peptidyl–tRNA slips (43). Consistent with the frameshifting data, all of the L3 basic thumb mutants promoted decreased affinity for aa-tRNA to the A-site (Figure 3A and B, and summarized in Table 1), but did not affect binding of Ac-aa-tRNA to the P-site (Figure 3C and D, summarized in Table 1). Specifically, R232A, which does not directly contact any rRNA bases, had the smallest effect on aa-tRNA binding (K_d values ∼126 nM compared to ∼94 nM for wild-type, i.e. 1.4-fold increase), while the K236A and K237A mutants, which participate in only a few rRNA contacts (Figure 4B), had moderate effects (∼165 nM each, 1.8-fold wild-type). In contrast, R247A, which contacts both H61 and H90 had a very strong effect on aa-tRNA binding (∼300 nM, 3.3-fold wild-type). The double mutants, which also affected multiple rRNA contacts had comparable effects on aa-tRNA binding (from ∼245 nM to ∼340 nM).

Eukaryotic elongation factor 2 (eEF2) catalyzes translocation and binds to the same site as the aa-tRNA–eEF1A–GTP ternary complex. Given the effects of the mutants on aa-tRNA binding, the effects of seven mutants on eEF2 binding were assayed (Figure 3E and F, summarized in Table 1). For wild-type ribosomes, the dissociation constant for eEF2 was $\sim 383 \pm 93$ nM. Similar values were observed for R232A, K236A and K237A mutant ribosomes, but the R247A mutant promoted an ∼8-fold increase in affinity for eEF2 ($K_d \sim 47$ nM). Among the double mutants assayed, the K237A/K236A mutant promoted the largest increase in affinity for eEF2 (∼84 nM, ∼4.5-fold increase), followed by K236A/R247A (∼110 nM, ∼3.5-fold increase), and K241A/R244A (∼229 nM, ∼1.7-fold increase).

Single round assays of peptidyltransferase activity were performed on puromycin treated salt washed ribosomes pre-loaded with Ac- [^{14}C]Phe-tRNA^{Phe} and purified through glycerol cushions (Complex C) as described in the 'Materials and Methods' section. The observed $K_{obs} = 0.34\ min^{-1}$ in wild-type ribosomes (Figure 3G, Table 1) is comparable to similar reactions using *E. coli* ribosomes and the Ac-Phe-tRNA substrate (44), confirming that these relatively low rates are determined by Ac-Phe-tRNA as a poor substrate for the peptidyltransferase reaction, and thus represent true measurements of peptidyltransferase activity, as opposed to peptidyl-tRNA turnover or other artifacts. The R232A, K236A and R247A mutants all promoted decreased rates of peptidyltransfer to approximately two–thirds of wild-type levels, while the double mutants (K236A/K237A, K236A/R1247A, and R247A/K248A) had stronger effects, decreasing rates to ∼50% of wild-type (Figure 3G and H, Table 1). Unexpectedly, the K237A mutant enhanced the rate of peptidyltransfer by almost 2-fold above wild-type levels.

The L3 basic thumb mutants promote changes in 25S rRNA structure both locally and in elements associated with aa-tRNA and eEF2 related functions

Inspection of atomic resolution ribosome structures reveals that the L3 basic thumb participates in a highly conserved set of interactions with the PTC proximal bases of Helix 73, and Helix 90, with bases on both sides of Helix 61, and with bases in a complex loop structure connecting Helices 61–64 of the LSU rRNA (Figures 1C, 4B and D) (6,36,45–47). Strikingly, while 2D maps of the LSU suggest that these structural elements are in physically separate domains from one another in (Figure 4B), the 3D structures reveal that the peptidyltransferase center, Helices 73, 90 and 94 are complexly folded to form a roughly Y-shaped topology, while the Helix 61–64 loop forms a cagelike structure opposite of this Y, with the L3 basic thumb positioned in the center where all of the basic side chains seem to glue all of the rRNA pieces together (Figures 1C, 4B and C). Importantly, the distal tip of Helix 92 is folded back upon itself where G2922 in the A-loop participates with C2876 and G2951 at the base of H90 to form an

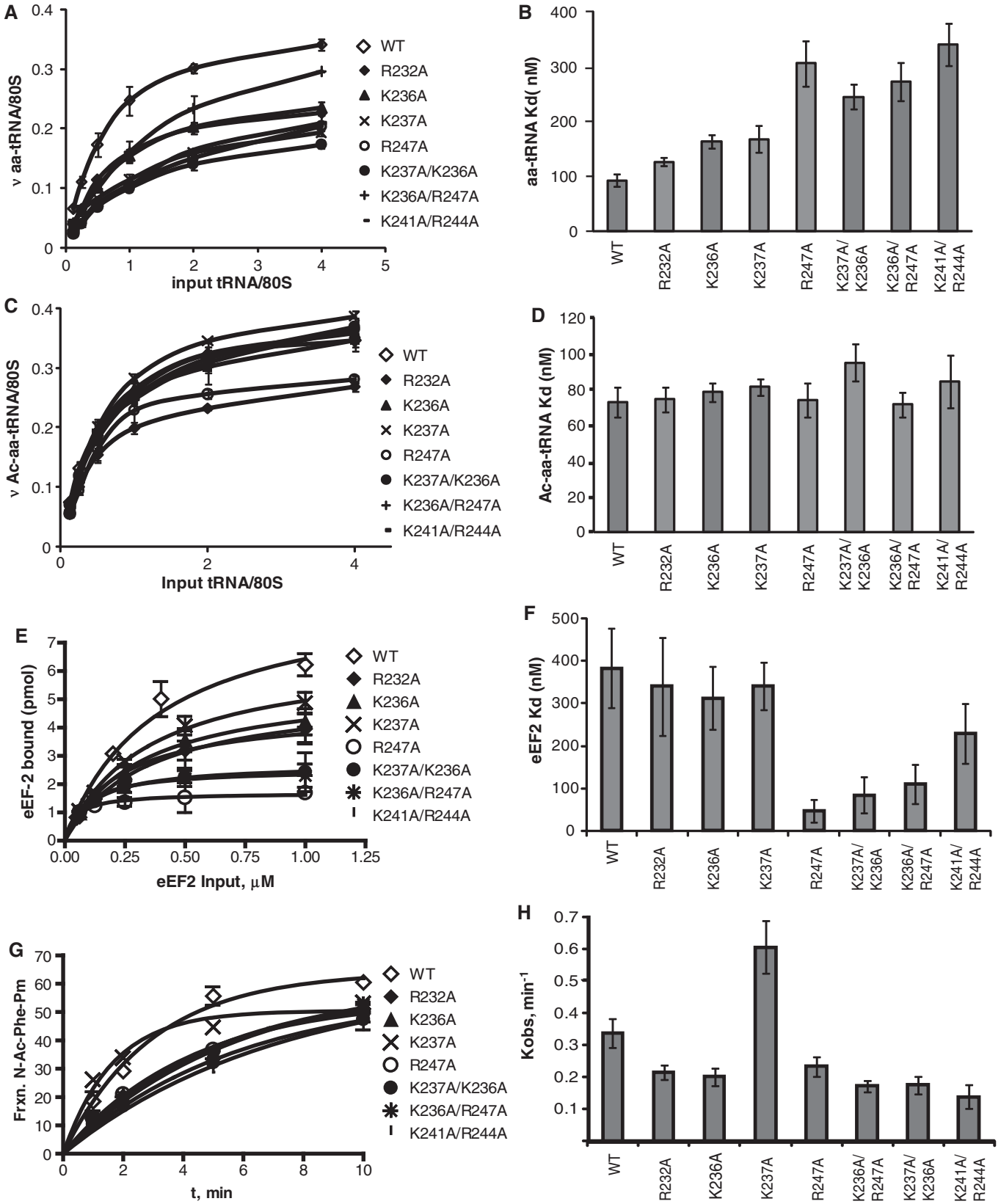

Figure 3. Biochemical characterization of ribosomes expressing L3 basic thumb mutants. (**A**) Single site isotherms of eEF1A stimulated binding of [^{14}C]Phe-tRNA^{Phe} to A-sites of poly(U) primed ribosomes pre-loaded with tRNA^{Phe} in their P-sites. (**B**) Dissociation constants calculated from data shown in (A). (**C**) Single site isotherms of Ac-[^{14}C]Phe-tRNA^{Phe} to P-sites of poly(U) primed ribosomes. (**D**) Dissociation constants calculated from data shown in (C). (**E**) eEF2-binding isotherms for wild-type and mutant ribosomes. (**F**) Dissociation constants calculated from data shown in (E). (**G**) Ac-[^{14}C]Phe-puromycin formation is plotted as percent of bound donor reacted. (**H**) Rates of peptidylpuromycin formation (K_{obs}) were calculated from data shown in (G).

A-minor motif in the A-site of the peptidyltransferase center (48). For ease of comparison, yeast 25S rRNA bases are listed with their *E. coli* homologs in Table 2.

To assess the effects of the viable mutants on rRNA structure, SHAPE [Selective 2′-Hydroxyl Acylation and Primer Extension, (34,49)] using 1M7 [1-methyl-7-nitroisatoic anhydride, (50)] was used to probe wild-type and selected mutant ribosomes containing either Ac-aa-tRNA^{Phe} at the P-site alone, or both tRNA^{Phe} and aa-tRNA^{Phe} at the P-and A-sites respectively (Figure 4). Inspection of the results revealed two general trends. First, that the mutants promoted significant changes in rRNA structure in the peptidyltransferase center (U2953, U2955, G2977), along the path taken by aa-tRNA as it accommodates into the LSU (accommodation corridor, G2912, U2924, C2929, A2934), in Helix 94 where it interacts with the globular domain of L3 (G3003, A3006, G3009), and in Helix 95 (U3019, U3023, A3033). Secondly, while the mutants only altered the Helix 73–Helix 95 region when only the P-site was occupied by Ac-aa-tRNA, the majority of changes in the Helix 91–93 region were observed when both A- and P-sites were occupied. Detailed analyses reveal that the R247A mutant conferred the largest number of changes in rRNA structure, promoting deprotection of C2985 in Helix 91, G3003, A3006, G3009 in Helix 94, and U3019, U3023 and A3033 in Helix 95 when only the P-site was occupied (Figure 4A and B). In contrast, this mutant promoted increased deprotection of G2912 in Helix 92, U2924 in the A-loop, A2934 in the bulge between Helix 92 and Helix 90, and U2955 in the peptidyltransferase center when the A-site was occupied by aa-tRNA. This mutant also caused hyperprotection of A2987 in Helix 73 when the A-site was occupied. Some of the other mutants had similar effects on some but not all of the same bases, e.g. K237A caused deprotection of G2912 and U2955, and enhanced protection of A2987 when the A-site was occupied. Other mutant specific effects were observed. For example, when only the P-site was occupied K247A promoted enhanced protection of G2977, while both K247A and K236A promoted deprotection of A2995 and U2953 under these conditions (Figure 4A and B). K237A also promoted increased protection from 1M7 at G2977 when both the A- and P-sites were occupied. R232A had significant effects in the 3′ loop between H90 and H92, and in the peptidyltransferase center (U2955). The observation that the bulged A2971 in Helix 93 was generally deprotected when only the P-site was occupied by Ac-aa-tRNA^{Phe}, but became protected from chemical attack upon loading of aa-tRNA^{Phe} into the A-site (Figure 4) serves as an important control, as this site occupancy-specific conformational change has also been observed for bacterial ribosomes (51). Interestingly, this pattern was also observed for A2926 in the A-loop, the possible significance of which is discussed below.

DISCUSSION

How is information flow coordinated through the ribosome to ensure the directionality of protein synthesis? Although the bulk of the ribosome is comprised of rRNA, and indeed, many of its critical functions are mediated through RNA–RNA interactions, it is clear that protrusions of ribosomal proteins, which can be thought of as loops, hooks and fingers, function to help 'switch' the ribosome between different conformational/functional states. For example, the C-terminal extension of *E. coli* S13 is thought to help coordinate movement of the peptidyl–tRNA with structural rearrangements at the ribosome interface that are critical for translocation by sampling the tRNA occupancy status at the decoding center (52,53). The N-terminal 'hook' of yeast L10 (*E. coli* L16) is believed to play an active role to coordinate switching of the ribosome between the pre- and post-translocational states (16). Ribosomal protein L2, which is intimately intertwined with multiple domains of the LSU, is thought to coordinate long range interactions between tRNAs and the ribosome (14). Ribosomal protein L3 is of particular interest because of its function as a 'gatekeeper' to the ribosomal A-site (13). A follow-up study suggested that two critical structures of L3, the W-finger and the N-terminal extension, function together as a 'rocker switch' to coordinate LSU associated functions (17). The L3 basic thumb is of interest because it appears to provide the structural link in this rocker switch mechanism. Protruding roughly perpendicular from the L3 W-finger toward the intersubunit face of the LSU, it is surrounded by a cagelike structure formed by a large bulge framed between Helices H61–64, Helix 73, Helix 90 and Helix 94. It is in the center of a nexus connecting the W-finger with the L3 globular domain, the peptidyltransferase center, the aa-tRNA accommodation corridor, and the SRL. Furthermore, it is proximal to the B5 intersubunit bridge, which involves multiple contacts involving bases in Helices 62 and 64 (54).

Unlike the small subunit (SSU), where the four rRNA domains are largely physically distinct, the six rRNA domains of the LSU are highly intertwined (54). With regard to the current study, the loop bounded by Helices 61–64 lie in domain IV, the PTC and Helices 90–93 and Helix 73 are in domain V, and Helices 94 and 95 are in domain IV. Previously, we demonstrated that the conformationally dynamic nature of the W-finger enables the central extension of L3 to function like a lever, and as such contribute to allosteric repositioning of rRNA structural elements (13,17). However, it was not clear how a small radial movement of thin, essentially planer element, could have such large and long ranging effects on rRNA structure and ribosome function. The perpendicular orientation of the basic thumb may answer this: we propose that it amplifies the action of this lever by adding three-dimensionality to the central extension in the form of a platform upon which structural elements from three different domains of 25S rRNA are anchored. In support of this, comparison of the L3 structures between EF-Tu and EF-G bound *Thermus thermophilus* ribosomes (55) reveals displacement of the α-carbon backbone of the W-finger and basic thumb structures by ~2–3 Å, and of some individual sidechains by as much as 5 Å (Supplementary Figure S1). This model explains how

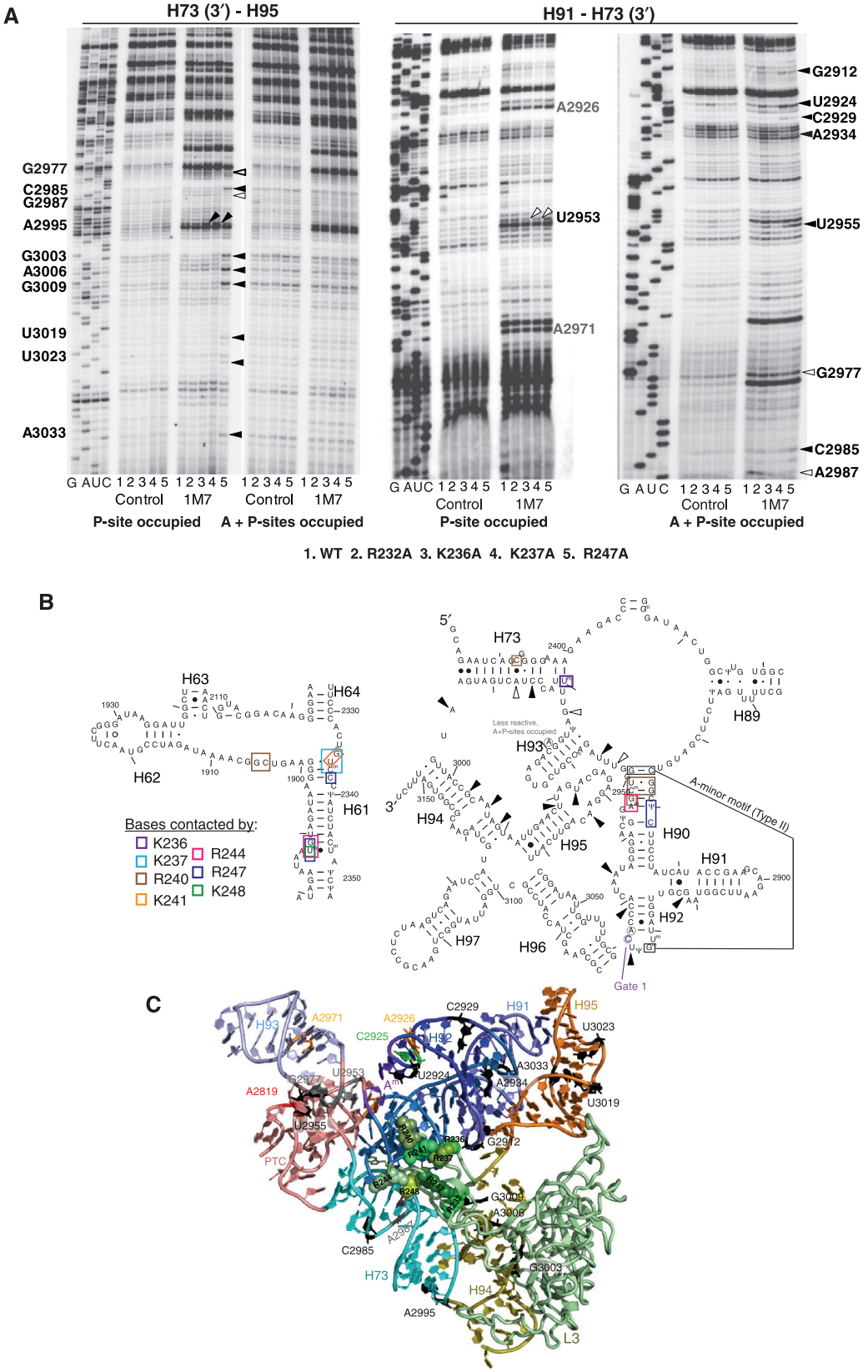

Figure 4. rRNA structure probing of wild-type and L3 basic thumb mutant ribosomes. (**A**) Poly(U) primed salt-washed ribosomes were either loaded with Ac-Phe-tRNA^{Phe} (P-site occupied) or tRNA^{Phe}+ Phe-tRNA^{Phe} (A + P-site occupied). Ribosomes were unmodified (control) or treated with 1M7 as indicated. Reverse transcriptase primer extension reactions spanned sequences from the 3′ half of Helix 73 through Helix 96 (left panel), or from Helix 91 through the 3′ half of Helix 73 (right panel). Sequencing reactions (left sides of panels) are labeled corresponding to the rRNA sense strand. Nucleotides whose 2′OH riboses were protected from 1M7 modification in mutant relative to wild-type ribosomes of are indicated by white

continued

the L3 central extension can have significant effects on coordinating the flow of information among the critical functional centers of the LSU, as well as to the SSU.

The large number of basically charged amino acids in the basic thumb enables it to participate in numerous hydrogen bonding/electrostatic interactions with rRNA bases, phosphates and riboses, functioning as a 'molecular clamp' to bridge these three domains. The current study focusing on eight amino acids in the L3 basic thumb neutralized their positive charges with alanine substitutions both singly and in selected pairs. The lethality of the R240A mutant as the sole form of L3 indicates that it may function to 'glue' the PTC proximal stem of H90 with the H61-H64 loop, and may well aid in coordinating formation of the C2876-G2922-G2951 A-minor motif that is critical for the 'induced fit' function of the peptidyltransferase center (5,6). Similarly, R247, which bridges Helix 61 with Helix 90 had profound effects on rRNA structure, ribosome biochemistry, translational fidelity, and cell growth, suggesting that it too is a critical bridging component between these two domains. Interestingly, the R247A/R248A double mutant was lethal, while R248A had a wild-type phenotype. This confirms the role of R247 and also indicates that the molecular defect conferred by the R247A single mutant might be partially complemented by the positively charged R248 adjacent to it. R240A and R247A appear to be the exception rather than the rule however, as the other single mutants had significantly lesser effects on these parameters. This is consistent with mutagenesis studies on other residues of L3, and with other LSU proteins and rRNA bases (11–15,17,23,56–57), suggesting that the ribosome is an elegantly evolved molecular machine containing multiple levels of functional redundancy. Furthermore, all of the double mutants tested had strong effects on binding of aa-tRNA and eEF2, and on peptidyltransfer (Figure 3), suggesting that it multiple defects are generally required to disrupt the functionally redundant interactions between the basic thumb and the LSU rRNA. As an aside, the observation that A2926 (base paired to U2920) was protected from 1M7 modification in wild-type ribosomes when both A- and P-sites were occupied by tRNAs but deprotected when only the P-site was occupied (Figure 4A) is unique to yeast. To our knowledge, this has not been observed in *E. coli* ribosomes (51), which contains a G-C base pair (C2551-G2557) at this position, a conformational difference that suggests a potentially novel antibiotic target. Interestingly, *Haloarcula marismortui* appears to split the difference with a G-U base pair (U2576-G2582).

Some specific changes in rRNA structure are particularly telling. The base stack of aa-tRNA C74 with *H. marismortui* U2590 (*E. coli* U2555, yeast U2924) is thought to promote the induced fit of peptidyltransfer (6). The enhanced deprotection of this base in R247A mutant ribosomes when both A- and P-sites were occupied by tRNAs is consistent with its strong effect on peptidyltransferase activity by this mutation (Figure 3 H). Interestingly, this base was also strongly deprotected under the same conditions in K237A mutant ribosomes, but in this case peptidyltransferase activity as monitored using the puromycin reaction was actually enhanced (Figure 3H). The rates of peptidyltransfer

Table 2. Homologous yeast 25S rRNA and *E. coli* 23S rRNA bases pertinent to this study

Yeast 25S rRNA base	*E. coli* 23S rRNA base
U1887$^{2'O–Me}$, G1888 (R244, R247, K248)	C1656, U1657
C1904, G1905 (R240)	A1671, 11672
G2325, U2326, C2327$^{2'O–Me}$ (K237, K241)	G1992, U1993, C1994
C2328 (R247)	U1995
C2392 (R240)	C2050
A2820	A2451 (PTC)
C2876	C2507 (A^m motif)
G2877 (R240)	C2508
C2878 (R240)	G2509
Ψ2880, C2881 (R247)	U2511, C2512
G2912	G2543
G2922$^{2'O–Me}$	G2553 (A^m motif)
U2924	U2555
C2925	C2556 (Gate 1)
C2929	A2560
A2934	A2564
A2946$^{2'O–Me}$ (R244)	A2577
G2947 (R244, R240)	G2578
C2848$^{2'O–Me}$, U2949 (R240)	C2579, Ψ2580
G2951	G2582
U2954	U2584
U2956	U2586
A2971	A2602
G2977	G2608
U2980$^{2'O–Me}$ (K236)	C2611
C2985	C2616
A2987	G2618
A2995	C2626
G3003	C2626
A3006	A2639
G3009	G2642
U3019	C2652
U3023	U2656
A3033	C2666

Contacts with specific L3 basic thumb amino acid side chains are indicated in parentheses. Superscript 2′O-Me indicates that 2′O-methylated bases. Ψ indicates pseudouridine.

Figure 4. Continued
arrowheads, and those deprotected relative to wild-type are indicated by black arrowheads. Bases marked in gray (A2926 and A2971) were deprotected when the A-site is unoccupied relative to when it contains aa-tRNA. **(B)** rRNA protection patterns of the L3 basic thumb mutants mapped onto the 2D diagram of 25S rRNA. Arrowheads indicate relatively protected and deprotected bases as above. Colored boxes indicate bases that interact with specified L3 basic thumb amino acid side chains. A2926 and A2971 are circled in gray, and C2925, which is the first gate in the aa-tRNA accommodation corridor, is circled in purple. The three bases participating the Type II A-minor motif that stabilizes the PTC are boxed and indicated. **(C)** Data from panels A and B mapped onto the 3D structure of the yeast ribosome. Indicated bases colored black correspond to bases deprotected in the mutants, while those colored gray are hyperprotected. Bases participating in the Type II A-minor motif (A^m) are colored purple. Helical structures and the PTC are color coded as indicated. Note that the loop formed between H61–H64 was removed from this figure because it obscures the L3 basic thumb.

observed in the current study ($\sim$0.3 min^{-1}) and in similar analyses using *E. coli* ribosomes are significantly lower than naturally occurring rates [estimated to be >300 s^{-1}, (58)] because Ac-Phe-tRNA is a poor substrate for this reaction. However, this property actually enables us to tease out the effects of local structural changes on PTC activity. Recent molecular dynamics simulations of portions of the ribosome reveal that individual bases can undergo a conservable degree of structural mobility due to local Brownian movements [reviewed in (59)], suggesting that specific bases in the PTC are relatively free to assume either the induced or uninduced conformations in the absence of tRNAs, and that the equilibrium between these two states is influenced by the presence or absence of aa-tRNA in the A-site. Thus, we suggest that R247A mutant drives this equilibrium toward the uninduced conformation, while the K237A mutant favors the induced arrangement. The observation of distinctly different patterns of rRNA protection/deprotection (e.g. compare G2912, C2929, U2953, G2977, C2985, A2995, G3003, A3006, G3009, U3019, U3023 and A3033 between the K237A and R247A mutants in Figure 4A) is consistent with the idea that they also have opposing effects on PTC conformation and functionality. In addition, early studies demonstrated that while empty ribosomes are heterogeneous in their affinity for eEF2, consisting of two sub-populations having K_d's for eEF2 ranging from subnanomolar to hundreds of nanomoles (60), the affinity for eEF2 strongly depends on the functional status of the ribosome as determined by the occupancy status of the A- and P-sites (61,62). This suggests that the R247A and the double mutants that increased eEF2 affinity shift this equilibrium as well, possibly stabilizing ribosomes in the pre-translocation state, and that the interactions between the 25S rRNA bases and L3 amino acid residues investigated here are involved in transitions between the pre- and post-translocational states.

As discussed above, the effects of the K237A mutant are locally confined to the PTC, while those conferred by R247A are more global. The latter is reflected in their different effects on ligand binding to the A-site: R247A promoted very strong effects on both aa-tRNA and eEF2 binding as compared to the much weaker effects conferred by K237A. Examination of the ligand binding data reveals a reciprocal relationship between affinities for aa-tRNA and eEF2, i.e. increased aa-tRNA K_d correlates with decreased eEF2 K_d (Figure 3). This is consistent with the model that L3 plays a central role as an allosteric switch to coordinate binding of elongation factors, opening and closing of the accommodation corridor, and PTC activity to ensure the unidirectionality of protein synthesis (13,17). Interestingly, all of the mutants affected peptidyltransfer, consistent with observations that this process is highly sensitive to even minor structural changes in the ribosome [reviewed in (63)].

In the end, the most important parameter is life; i.e. how does the L3 basic thumb contribute to the fitness of the organism? While only some of the mutants had gross effects on cell growth, they all affected translational fidelity as monitored by decreased rates of −1 PRF (Figure 2). In fact, the effects on −1 PRF correlated well with the A-site aa-tRNA-binding data. For example, R247A and K241A/R244A, which had the most pronounced effects on −1 PRF, also promoted >3-fold decreases in affinity for aa-tRNA. In contrast, R232A and K236A, which had the smallest effects on aa-tRNA binding, also promoted the smallest decreases in −1 PRF. As noted above, the mutants investigated in this report are unique in that they are the first examples that promoted decreased −1 PRF. This trend had only previously been observed with anisomycin, a competitive inhibitor for aa-tRNA 3′ binding to the PTC (41). We have suggested that the majority of −1 PRF occurs after aa-tRNA accommodation into the A-site, and prior to peptidyltransfer, while a smaller fraction can occur during translocation [reviewed in (64)], a view that is supported by a recent study coupling kinetic modeling of −1 PRF within the translation elongation cycle with mass spectroscopic analyses of frameshifted peptide products (P.-Y. Liao *et al.*, submitted for publication). By this model, decreased rates of aa-tRNA accommodation into the A-site should decrease the steady state abundance of substrate for −1 PRF, thus inhibiting this reaction. Changes in −1 PRF in turn alter the relative amounts of viral protein products available for viral particle self assembly, a ratio that is critical for virus propagation (18,40). This illustrates how minute changes in ribosome structure at the atomic scale can propagate outward, affecting ribosome biochemistry, translational fidelity, and the ability of cells to replicate viruses.

SUPPLEMENTARY DATA

Supplementary Data are available at NAR Online.

ACKNOWLEDGEMENTS

The authors would like to thank members of the Dinman laboratory for their critical input and helpful suggestions. We would also like to thank Kevin Weeks for the kind gift of 1M7.

FUNDING

National Institutes of Health (5 R01 GM058859; to J.D.D.); American Heart Association (AHA 0630163N; to A.M). Funding for open access charge: National Institutes of Health (5 R01 GM058859); American Heart Association (AHA 0630163N).

Conflict of interest statement. None declared.

REFERENCES

1. Dunkle,J.A. and Cate,J.H. (2010) Ribosome structure and dynamics during translocation and termination. *Annu. Rev. Biophys.*, **39**, 227–244.

2. Rodnina,M.V. and Wintermeyer,W. (2001) Fidelity of aminoacyl-tRNA selection on the ribosome: kinetic and structural mechanisms. *Annu. Rev. Biochem.*, **70**, 415–435.
3. Walker,S.E., Shoji,S., Pan,D., Cooperman,B.S. and Fredrick,K. (2008) Role of hybrid tRNA-binding states in ribosomal translocation. *Proc. Natl Acad. Sci. USA*, **105**, 9192–9197.
4. Aitken,C.E., Petrov,A. and Puglisi,J.D. (2010) Single ribosome dynamics and the mechanism of translation. *Annu. Rev. Biophys.*, **39**, 491–513.
5. Schmeing,T.M., Huang,K.S., Strobel,S.A. and Steitz,T.A. (2005) An induced-fit mechanism to promote peptide bond formation and exclude hydrolysis of peptidyl-tRNA. *Nature*, **438**, 520–524.
6. Simonovic,M. and Steitz,T.A. (2008) Peptidyl-CCA deacylation on the ribosome promoted by induced fit and the O3'-hydroxyl group of A76 of the unacylated A-site tRNA. *RNA.*, **14**, 2372–2378.
7. Voorhees,R.M., Weixlbaumer,A., Loakes,D., Kelley,A.C. and Ramakrishnan,V. (2009) Insights into substrate stabilization from snapshots of the peptidyl transferase center of the intact 70S ribosome. *Nat. Struct. Mol. Biol.*, **16**, 528–533.
8. Whitford,P.C., Geggier,P., Altman,R.B., Blanchard,S.C., Onuchic,J.N. and Sanbonmatsu,K.Y. (2010) Accommodation of aminoacyl-tRNA into the ribosome involves reversible excursions along multiple pathways. *RNA.*, **16**, 1196–1204.
9. Yusupova,G., Jenner,L., Rees,B., Moras,D. and Yusupov,M. (2006) Structural basis for messenger RNA movement on the ribosome. *Nature*, **444**, 391–394.
10. Brunelle,J.L., Shaw,J.J., Youngman,E.M. and Green,R. (2008) Peptide release on the ribosome depends critically on the 2' OH of the peptidyl-tRNA substrate. *RNA.*, **14**, 1526–1531.
11. Rakauskaite,R. and Dinman,J.D. (2006) An arc of unpaired "hinge bases" facilitates information exchange among functional centers of the ribosome. *Mol. Cell Biol.*, **26**, 8992–9002.
12. Baxter-Roshek,J.L., Petrov,A.N. and Dinman,J.D. (2007) Optimization of ribosome structure and function by rRNA base modification. *PLoS ONE*, **2**, e174.
13. Meskauskas,A. and Dinman,J.D. (2007) Ribosomal protein L3: gatekeeper to the A-site. *Mol. Cell*, **25**, 877–888.
14. Meskauskas,A., Russ,J.R. and Dinman,J.D. (2008) Structure/function analysis of yeast ribosomal protein L2. *Nucleic Acids Res.*, **36**, 1826–1835.
15. Rakauskaite,R. and Dinman,J.D. (2008) rRNA mutants in the yeast peptidyltransferase center reveal allosteric information networks and mechanisms of drug resistance. *Nucleic Acids Res.*, **36**, 1497–1507.
16. Petrov,A.N., Meskauskas,A., Roshwalb,S.C. and Dinman,J.D. (2008) Yeast ribosomal protein L10 helps coordinate tRNA movement through the large subunit. *Nucleic Acids Res.*, **36**, 6187–6198.
17. Meskauskas,A. and Dinman,J.D. (2008) Ribosomal protein L3 functions as a 'rocker switch' to aid in coordinating of large subunit-associated functions in eukaryotes and Archaea. *Nucleic Acids Res.*, **36**, 6175–6186.
18. Dinman,J.D. and Wickner,R.B. (1992) Ribosomal frameshifting efficiency and Gag/Gag-pol ratio are critical for yeast M_1 double-stranded RNA virus propagation. *J. Virol.*, **66**, 3669–3676.
19. Meskauskas,A., Harger,J.W., Jacobs,K.L.M. and Dinman,J.D. (2003) Decreased peptidyltransferase activity correlates with increased programmed -1 ribosomal frameshifting and viral maintenance defects in the yeast *Saccharomyces cerevisiae*. *RNA*, **9**, 982–992.
20. Harger,J.W. and Dinman,J.D. (2003) An *in vivo* dual-luciferase assay system for studying translational recoding in the yeast *Saccharomyces cerevisiae*. *RNA*, **9**, 1019–1024.
21. Jacobs,J.L. and Dinman,J.D. (2004) Systematic analysis of bicistronic reporter assay data. *Nucleic Acids Res.*, **32**, e160–e170.
22. Von der Haar,F. (1979) Purification of aminoacyl-tRNA synthetases. *Methods Enzymol.*, **59**, 257–267.
23. Meskauskas,A., Petrov,A.N. and Dinman,J.D. (2005) Identification of functionally important amino acids of ribosomal protein L3 by saturation mutagenesis. *Mol. Cell Biol.*, **25**, 10863–10874.
24. Walker,S.E. and Fredrick,K. (2008) Preparation and evaluation of acylated tRNAs. *Methods*, **44**, 81–86.
25. Triana-Alonso,F.J., Spahn,C.M., Burkhardt,N., Rohrdanz,B. and Nierhaus,K.H. (2000) Experimental prerequisites for determination of tRNA binding to ribosomes from Escherichia coli. *Methods Enzymol.*, **317**, 261–276.
26. Leshin,J.A., Rakauskaite,R., Dinman,J.D. and Meskauskas,A. (2010) Enhanced purity, activity and structural integrity of yeast ribosomes purified using a general chromatographic method. *RNA Biol.*, **7** [Epub ahead of print 22 May, doi:10.4161/rna].
27. Dresios,J., Panopoulos,P., Frantziou,C.P. and Synetos,D. (2001) Yeast ribosomal protein deletion mutants possess altered peptidyltransferase activity and different sensitivity to cycloheximide. *Biochemistry*, **40**, 8101–8108.
28. Synetos,D. and Coutsogeorgopoulos,C. (1987) Studies on the catalytic rate constant of ribosomal peptidyltransferase. *Biochim. Biophys. Acta*, **923**, 275–285.
29. Dresios,J., Derkatch,I.L., Liebman,S.W. and Synetos,D. (2000) Yeast ribosomal protein L24 affects the kinetics of protein synthesis and ribosomal protein L39 improves translational accuracy, while mutants lacking both remain viable. *Biochemistry*, **39**, 7236–7244.
30. Ortiz,P.A., Ulloque,R., Kihara,G.K., Zheng,H. and Kinzy,T.G. (2006) Translation elongation factor 2 anticodon mimicry domain mutants affect fidelity and diphtheria toxin resistance. *J. Biol. Chem.*, **281**, 32639–32648.
31. Pappenheimer,A.M. Jr (1977) Diphtheria toxin. *Annu. Rev. Biochem.*, **46**, 69–94.
32. Gill,D.M. and Dinius,L.L. (1973) The elongation factor 2 content of mammalian cells. Assay method and relation to ribosome number. *J. Biol. Chem.*, **248**, 654–658.
33. Gill,D.M., Pappenheimer,A.M. Jr and Baseman,J.B. (1969) Studies on transferase II using diphtheria toxin. *Cold Spring Harb. Symp. Quant. Biol.*, **34**, 595–602.
34. Wilkinson,K.A., Merino,E.J. and Weeks,K.M. (2006) Selective 2′-hydroxyl acylation analyzed by primer extension (SHAPE): quantitative RNA structure analysis at single nucleotide resolution. *Nat. Protoc.*, **1**, 1610–1616.
35. Rheinberger,H.J., Geigenmuller,U., Wedde,M. and Nierhaus,K.H. (1988) Parameters for the preparation of Escherichia coli ribosomes and ribosomal subunits active in tRNA binding. *Methods Enzymol.*, **164**, 658–670.
36. Taylor,D.J., Devkota,B., Huang,A.D., Topf,M., Narayanan,E., Sali,A., Harvey,S.C. and Frank,J. (2009) Comprehensive molecular structure of the eukaryotic ribosome. *Structure*, **17**, 1591–1604.
37. Wickner,R.B. (1996) Double-stranded RNA viruses of *Saccharomyces cerevisiae*. *Microbiol. Rev.*, **60**, 250–265.
38. Dinman,J.D., Icho,T. and Wickner,R.B. (1991) A -1 ribosomal frameshift in a double-stranded RNA virus forms a Gag-pol fusion protein. *Proc. Natl Acad. Sci. USA*, **88**, 174–178.
39. Wickner,R.B., Porter-Ridley,S., Fried,H.M. and Ball,S.G. (1982) Ribosomal protein L3 is involved in replication or maintenance of the killer double-stranded RNA genome of *Saccharomyces cerevisiae*. *Proc. Natl Acad. Sci. USA*, **79**, 4706–4708.
40. Plant,E.P., Rakauskaite,R., Taylor,D.R. and Dinman,J.D. (2010) Achieving a golden mean: mechanisms by which coronaviruses ensure synthesis of the correct stoichiometric ratios of viral proteins. *J. Virol.*, **84**, 4330–4340.
41. Dinman,J.D., Ruiz-Echevarria,M.J., Czaplinski,K. and Peltz,S.W. (1997) Peptidyl transferase inhibitors have antiviral properties by altering programmed -1 ribosomal frameshifting efficiencies: development of model systems. *Proc. Natl Acad. Sci. USA*, **94**, 6606–6611.
42. Jacks,T., Power,M.D., Masiarz,F.R., Luciw,P.A., Barr,P.J. and Varmus,H.E. (1988) Characterization of ribosomal frameshifting in HIV-1 *gag-pol* expression. *Nature*, **331**, 280–283.
43. Kawakami,K., Paned,S., Faioa,B., Moore,D.P., Boeke,J.D., Farabaugh,P.J., Strathern,J.N., Nakamura,Y. and Garfinkel,D.J. (1993) A rare tRNA-Arg(CCU) that regulates Ty*1* element ribosomal frameshifting is essential for Ty*1* retrotransposition in *Saccharomyces cerevisiae*. *Genetics*, **135**, 309–320.
44. Sharma,D., Southworth,D.R. and Green,R. (2004) EF-G-independent reactivity of a pre-translocation-state ribosome complex with the aminoacyl tRNA substrate

puromycin supports an intermediate (hybrid) state of tRNA binding. *RNA*, **10**, 102–113.
45. Selmer,M., Dunham,C.M., Murphy,F.V., Weixlbaumer,A., Petry,S., Kelley,A.C., Weir,J.R. and Ramakrishnan,V. (2006) Structure of the 70S ribosome complexed with mRNA and tRNA. *Science*, **313**, 1935–1942.
46. Korostelev,A., Trakhanov,S., Laurberg,M. and Noller,H.F. (2006) Crystal structure of a 70S ribosome-tRNA complex reveals functional interactions and rearrangements. *Cell*, **126**, 1065–1077.
47. Jenner,L., Rees,B., Yusupov,M. and Yusupova,G. (2007) Messenger RNA conformations in the ribosomal E site revealed by X-ray crystallography. *EMBO Rep.*, **8**, 846–850.
48. Nissen,P., Ippolito,J.A., Ban,N., Moore,P.B. and Steitz,T.A. (2001) RNA tertiary interactions in the large ribosomal subunit: the A-minor motif. *Proc. Natl Acad. Sci. USA*, **98**, 4899–4903.
49. Merino,E.J., Wilkinson,K.A., Coughlan,J.L. and Weeks,K.M. (2005) RNA structure analysis at single nucleotide resolution by selective 2′-hydroxyl acylation and primer extension (SHAPE). *J. Am. Chem. Soc.*, **127**, 4223–4231.
50. Mortimer,S.A. and Weeks,K.M. (2007) A fast-acting reagent for accurate analysis of RNA secondary and tertiary structure by SHAPE chemistry. *J. Am. Chem. Soc.*, **129**, 4144–4145.
51. Moazed,D. and Noller,H.F. (1989) Interaction of tRNA with 23S rRNA in the ribosomal A, P, and E sites. *Cell*, **57**, 585–597.
52. Cochella,L., Brunelle,J.L. and Green,R. (2007) Mutational analysis reveals two independent molecular requirements during transfer RNA selection on the ribosome. *Nat. Struct. Mol. Biol*, **14**, 30–36.
53. Cukras,A.R. and Green,R. (2005) Multiple effects of S13 in modulating the strength of intersubunit interactions in the ribosome during translation. *J. Mol. Biol.*, **349**, 47–59.
54. Yusupov,M.M., Yusupova,G.Z., Baucom,A., Lieberman,K., Earnest,T.N., Cate,J.H. and Noller,H.F. (2001) Crystal Structure of the Ribosome at 5.5 A Resolution. *Science*, **292**, 883–896.
55. Gao,Y.G., Selmer,M., Dunham,C.M., Weixlbaumer,A., Kelley,A.C. and Ramakrishnan,V. (2009) The structure of the ribosome with elongation factor G trapped in the posttranslocational state. *Science*, **326**, 694–699.
56. Kiparisov,S., Petrov,A., Meskauskas,A., Sergiev,P.V., Dontsova,O.A. and Dinman,J.D. (2005) Structural and functional analysis of 5S rRNA. *Mol Genet. Genom.*, **27**, 235–247.
57. Petrov,A., Meskauskas,A. and Dinman,J.D. (2004) Ribosomal protein L3: influence on ribosome structure and function. *RNA Biol.*, **1**, 59–65.
58. Bieling,P., Beringer,M., Adio,S. and Rodnina,M.V. (2006) Peptide bond formation does not involve acid-base catalysis by ribosomal residues. *Nat. Struct. Mol. Biol.*, **13**, 423–428.
59. Munro,J.B., Sanbonmatsu,K.Y., Spahn,C.M. and Blanchard,S.C. (2009) Navigating the ribosome's metastable energy landscape. *Trends Biochem. Sci.*, **34**, 390–400.
60. Nygard,O. and Nilsson,L. (1989) Characterization of the ribosomal properties required for formation of a GTPase active complex with the eukaryotic elongation factor 2. *Eur. J. Biochem.*, **179**, 603–608.
61. Nolan,R.D., Grasmuk,H. and Drews,J. (1975) The binding of tritiated elongation factors 1 and 2 to ribosomes from Krebs II mouse ascites tumor cells. *Eur. J. Biochem.*, **50**, 391–402.
62. Nombela,C. and Ochoa,S. (1973) Conformational control of the interaction of eukaryotic elongation factors EF-1 and EF-2 with ribosomes. *Proc. Natl Acad. Sci. USA*, **70**, 3556–3560.
63. Beringer,M. and Rodnina,M.V. (2007) The ribosomal peptidyl transferase. *Mol. Cell*, **26**, 311–321.
64. Dinman,J.D. and Berry,M.J. (2006) Regulation of Termination and Recoding. In Mathews,M.B., Sonenberg,N. and Hershey,J.W.B. (eds), *Translational Control in Biology and Medicine*. Cold Spring Harbor Press, Cold Spring Harbor, NY.